BIOLOGY OF REPRODUCTION (2015) **93**(3):78, 1–13
Published online before print 29 July 2015.
DOI 10.1095/biolreprod.115.128850

Left-Biased Spermatogenic Failure in 129/SvJ *Dnd1*$^{Ter/+}$ Mice Correlates with Differences in Vascular Architecture, Oxygen Availability, and Metabolites[1]

Ximena M. Bustamante-Marin,[3,4] Matthew S. Cook,[3,5] Jessica Gooding,[6] Christopher Newgard,[6] and Blanche Capel[2,3]

[3]*Department of Cell Biology, Duke University, Durham, North Carolina*
[4]*Departmento Biomédico, Facultad de Ciencias de la Salud, Universidad de Antofagasta, Antofagasta, Chile*
[5]*Department of Anatomy, University of California, San Francisco, California*
[6]*Sarah W. Stedman Nutrition and Metabolism Center & Duke Molecular Physiology Institute, Departments of Pharmacology and Cancer Biology & Medicine, Duke University Medical Center, Durham, North Carolina*

ABSTRACT

Homozygosity for the *Ter* mutation in the RNA-binding protein *Dead end 1* (*Dnd1*$^{Ter/Ter}$) sensitizes germ cells to degeneration in all mouse strains. In 129/SvJ mice, approximately 10% of *Dnd1*$^{Ter/+}$ heterozygotes develop spermatogenic failure, and 95% of unilateral cases occur in the left testis. The first differences between right and left testes were detected at Postnatal Day 15 when many more spermatogonial stem cells (SSCs) were undergoing apoptosis in the left testis compared to the right. As we detected no significant left/right differences in the molecular pathway associated with body axis asymmetry or in the expression of signals known to promote proliferation, differentiation, and survival of germ cells, we investigated whether physiological differences might account for asymmetry of the degeneration phenotype. We show that left/right differences in vascular architecture are associated with a decrease in hemoglobin saturation and increased levels of HIF-1alpha in the left testis compared to the right. In *Dnd1* heterozygotes, lower oxygen availability was associated with metabolic differences, including lower levels of ATP and NADH in the left testis. These experiments suggest a dependence on oxygen availability and metabolic substrates for SSC survival and suggest that *Dnd1*$^{Ter/+}$ SSCs may act as efficient sensors to detect subtle environmental changes that alter SSC fate.

Dnd1/*DND1, germ cell, hypoxia, metabolism, spermatogenic failure, spermatogonial stem cells*

INTRODUCTION

The global prevalence of male infertility is unknown; however, in 20% to 55% of couples seeking fertility assistance, the male partner is diagnosed with spermatogenic impairment [1, 2]. Multiple factors, including genetic defects and environmental influences, can affect spermatogenesis by disrupting spermatogonia or the surrounding somatic cells either during developmental stages or in adult life [3]. However, the underlying causes of spermatogenic failure remain uncharacterized in half of the cases [4].

In mammals, the amplification of the population of spermatogonial stem cells (SSCs) supports the continuous production of sperm in adult life. SSCs are derived from a small set of cells specified as primordial germ cells in the early embryo [5–7]. This group of pluripotent cells migrates through the developing embryo to reach the genital ridge between Embryonic Day 10.5 (E10.5) and E11.5 [8, 9]. There, in response to signals from the testicular somatic environment, including an early pulse of FGF9, germ cells proliferate and transiently upregulate Nodal and Cripto, which control the size and pluripotency of the future SSC population [10, 11]. Male gonocytes proliferate until ~E14.5, when they enter mitotic arrest in G1/G0 and undergo a series of epigenetic modifications that lead to their differentiation as prospermatogonia [12–14]. Just after birth, prospermatogonia exit G0 arrest and resume active cell cycle. Some undergo apoptosis while others migrate to the periphery of the seminiferous tubules to establish the definitive SSC population. This population maintains its numbers by symmetric divisions and also divides asymmetrically to give rise to differentiating spermatogonia throughout the male lifetime [15].

Over 200 mouse models carrying genetic mutations affecting various stages of germ cell development have been described [16]. Multiple growth factors produced by Sertoli cells, including *Cxcl12, Gdnf, KitL*, and *Fasl*, are necessary to establish and maintain the population of SSCs [17–20]. On the other hand, mice deficient for the gene *Bax,* a proapoptotic protein that induces cell death, also undergo testicular atrophy [21], suggesting that the success of spermatogenesis requires a balance between signals that promote and limit cell survival.

In 1973, Leroy Stevens described a new substrain of 129/Sv mice carrying a spontaneous mutation *Ter* [22]. In all genetic backgrounds, homozygous mutants show apoptotic loss of a large proportion of primordial germ cells beginning soon after their specification [23, 24]. In the 129/SvJ genetic background, germ cells that escape the initial wave of apoptosis frequently undergo spontaneous transformation into teratomas at the stage when male germ cells typically enter mitotic arrest (E13.5–E16.5) [22, 25].

In 1994, the *Ter* mutation was mapped to a region of chromosome 18 and later to a specific point mutation that introduced a premature stop codon in the dead-end homolog 1 gene (*Dnd1*^{Ter}) [26, 27]. *Dnd1* is expressed in keratinocytes [28] and intestine [29] and is required for survival of primordial germ cells [30]. It encodes an RNA-binding protein that can associate with the CNOT complex to regulate polyadenylation [31] and can protect target transcripts by binding to their 3′-

[1]Funding from the Lalor Foundation and Comisión Nacional de Investigación Científica y Tecnológica (CONICYT) Chile, to X.B.M., as well as from NIGMS to B.C.
[2]Correspondence: Blanche Capel, 0452 Nanaline Duke, Durham, NC 27710. E-mail: blanche.capel@duke.edu.

Received: 7 February 2015.
First decision: 6 March 2015.
Accepted: 6 July 2015.

eISSN: 1529-7268 http://www.biolreprod.org
ISSN: 0006-3363

untranslated regions, and antagonizing repression of translation mediated by microRNAs [32]. RNA immunoprecipitation experiments, using an antibody against a tagged DND1 protein, showed that DND1 binds transcripts of a group of negative regulators of the cell cycle [33]. Two of these, *p27* and *p21,* normally expressed during G0 in male germ cells [13], were not translated in *Dnd1*$^{Ter/Ter}$ mutants, providing a plausible explanation for the failure of most male germ cells to enter cell cycle arrest in homozygous mutants [33].

In 129/SvJ mice carrying a heterozygous mutation (*Dnd1*$^{Ter/+}$), the incidence of both teratoma and spermatogenic failure is much lower, and typically occurs unilaterally with a strong bias to the left testis. The left-sided bias in teratoma incidence and in spermatogenic failure was first described over 60 yr ago in wild-type 129/SvJ mice, which have a 1% incidence of teratoma [25]. Although the mechanism underlying this asymmetric phenotype has not been identified, Stevens showed that crossing the situs inversus viscerum mutation onto the 129/SvJ strain led to a reversal of the bias to the right testis in accordance with reversal of the asymmetry in the body axis [34]. This result suggested that the sidedness of spermatogenic failure in 129/SvJ *Dnd1*$^{Ter/+}$ mice is due to molecular or physiological differences that arise from body axis asymmetry.

Here, we show that spermatogenic failure in the left testis of 129/SvJ *Dnd1*$^{Ter/+}$ is evident as early as Postnatal Day 15 (P15) and is likely attributable to a left-sided increase in the number of apoptotic SSCs. This phenotype can be rescued by introducing a heterozygous mutation in the proapoptotic gene *Bax*. Because we detected no differences in the molecular pathway associated with body axis asymmetry or in the expression of genes that promote proliferation, differentiation, and survival of germ cells, we hypothesized that the bias in cell death arises from physiological differences that stem from left/right asymmetry in vascular architecture. We found subtle differences in the availability of oxygen in the left testis compared to the right, and lower oxygen availability was consistent with higher levels of HIF-1α and with metabolic differences measured in the left testis of *Dnd1* heterozygotes, including lower levels of ATP and NADH. We propose that heterozygosity for the *Dnd1*^{Ter} mutation sensitizes SSCs to subtle environmental influences and suggests a dependence on oxygen availability and/or metabolic substrates for SSC survival.

MATERIALS AND METHODS

Mice, Timed Matings, and Genotyping

Dnd1$^{Ter/+}$, *Oct4-EGFP* (enhanced green fluorescent protein), and *Bax*$^{+/-}$ mice were maintained on a 129/SvJ background, genotyped, and crossed as described previously [24]. For timed matings, males and females were placed together in the afternoon, and plugs found the following morning were counted as E0.5. All the animals were maintained and experiments were conducted according to Duke University Medical Center-Institutional Animal Care and Use Committee and National Institutes of Health guidelines.

Histology and Morphometric Analysis

Testes were fixed in Bouin for 6 h to overnight depending of their size. For samples older than P10, testes were gently punctured two to five times with a 27-gage needle. After 2 h of fixation, samples were cut in half with a scalpel and fixed overnight at room temperature. The samples were dehydrated in an alcohol series (70%, 80%, 90%, and 100%, 1 h each). The remaining water was removed with two rinses in VM&P Naphtha (Klean-Strip) for 1 h each. Samples were incubated overnight in a 1:1 solution of paraffin:naphta at 65°C, followed by three rinses in pure paraffin (McCormick Scientific) of 1 h each and embedded. Serial sections of 8 μm were placed on slides, rehydrated, and stained with hematoxylin (Lerner Laboratories) and eosin (Ricca Chemical Company) for morphological analysis and tubule diameter measurements. Using an Axioplan 2 microscope (Zeiss), five random images were taken of three sections in >20 right and left biological replicates for each stage (P15, P30, and P180). The diameter of the tubules in each image was estimated as the average of two perpendicular measurements using FIJI software. The data represent the mean (± SD). Statistical analysis was performed using the Student *t*-test.

Immunofluorescence

Fluorescent immunocytochemistry was performed in either whole mount right and left gonads at E11.5, whole-mount tubules at P8–P17, or frozen sections of right and left testes at P0 and later stages. E11.5 gonads expressing the *Oct4*-EGFP reporter were dissected in phosphate-buffered saline (PBS) and fixed in 4% paraformaldehyde (PFA) (Thermo Fisher Scientific) overnight at 4°C. For whole-mount tubules, P8–P17 right and left testes were dissected in PBS, the tunica was removed, and the testes were gently agitated in PBS to free tubules from the interstitial tissue. The tubules were teased apart and fragmented with fine forceps in a Petri dish. Fragments were collected in a 1.5 ml tube with fresh PBS. One-half of the tubule suspension was used for total RNA extraction and the other for immunofluorescence. After tubules settled to the bottom of the tube, the PBS was removed and replaced with Trizol for RNA extraction (see below) or fixed in 4% PFA overnight at 4°C for immunocytochemistry. For frozen sections, testes between P0 and later stages were fixed in 4% PFA overnight at 4°C. For stages older than P10, the testes were gently punctured two to five times with a 27-gage needle followed by 2 h in 4% PFA. After this brief fixation, samples (P10 and older) were cut in half with a scalpel and fixed for a further 5 h in PFA at 4°C. After several washes in PBS, the samples were processed for optimal cutting temperature (OCT, Sakura Finetek USA, Inc.) embedded through a sucrose gradient (10%, 15%, 20%, 20%: OCT [1:1] overnight at 4°C). Samples were cryosectioned at 16 μm. For antibody staining, all the samples were processed as follows: after several washes in PBS, samples were incubated in blocking solution (PBS plus 10% fetal bovine serum, 0.1% Triton X-100, and 3% bovine serum albumin [EMD Millipore]) for 1–2 h at room temperature or overnight at 4°C. Primary antibodies were diluted in blocking solution and incubated with samples overnight at 4°C. After several washes in washing solution (PBS plus 1% fetal bovine serum, 0.1% Triton X-100, and 3% bovine serum albumin), fluorescent secondary Cy5- or Cy3-conjugated (1:500 dilution; Jackson ImmunoResearch) or Alexa 647- or Alexa 488-conjugated (1:500 dilution; Molecular Probes Inc., Eugene, OR) antibodies were applied for 2 h at room temperature or overnight at 4°C. To stain nuclei, 4′,6-diamidino-2-phenylindole (Sigma-Aldrich) or SYTO13 (1:1000 dilution; Molecular Probes) was used. Samples were mounted in 2.5% 1,4-diazabicyclo[2.2.2] octane (Sigma-Aldrich) and imaged using a Zeiss 710 inverted confocal microscope.

The antibodies and dilutions used were: rabbit anti-SOX9 (ab5535, 1:2000 dilution; Millipore); rabbit anti-DDX4/MVH (ab13840, 1:500 dilution; Abcam); rabbit anti-Ki67 (RM-9106-S, 1:500 dilution; NeoMarkers); rabbit anti-STRA8 (kindly provided by Dr. Mike Griswold; 1:1000 dilution); goat anti-cKIT (AF1356, 1:100; R&D System); goat anti-GATA4 (sc-1237, 1:100 dilution; Santa Cruz); mouse anti-PLZF (OP128, 1:300 dilution; Calbiochem); rabbit anti-cCASPASE-3 (9661S, 1:500 dilution; Cell Signaling); rabbit anti-cPARP (9544P; Cell Signaling); rat anti-GCNA (kindly provided by Dr. George Enders; 1:100 dilution); mouse anti-TUJ1 (MMS-435P, 1:1000 dilution; Covance); and γH2AX (07-164, 1:500 dilution; Upstate).

Cell Counting

E11.5 gonads were imaged using a Zeiss 710 inverted confocal microscope. The number of OCT4-EGFP-positive cells were counted in 16 images from seven biological replicates (four optical sections in the Z plane for each of four sections in the X plane). To count the number of PLZF and cCASPASE-3-positive cells, six confocal images were taken of each biological replicate (n = 6 mice of each genotype). The number of positive cells was counted using the FIJI Software and normalized to a unit area of 1 mm^2 (image size was 375 μm × 375 μm). Statistical analysis was performed using the Student *t*-test.

Fluorescence-Activated Cell Sorting

E13.5 and E14.5 OCT4-EGFP+ right and left gonads were dissected, separated from the mesonephros, and individually collected in PBS on ice. Germ cells were sorted by fluorescence-activated cell sorting (FACS) as described previously [35]. EGFP-positive cells were collected in PBS and centrifuged at 3000 rpm for 5 min at 4°C to pellet the cells. The PBS was aspirated, and RNA extraction was performed.

RNA Extraction and Quantitative PCR

Total RNA was extracted using a TRIzol/isopropanol precipitation method for tubules from six individual right and left testes at P8 (isolated as described above) and FACS-based EGFP-positive cells collected from seven individual E13.5 and E14.5 testes. DNase treatment (18068-015; Invitrogen) was performed, and cDNA synthesis was carried out using the iScript kit (170-889; Bio-Rad) using 400–500 ng of total RNA. Quantitative RT-PCR (qPCR) was used to determine relative expression levels of transcripts in right and left gonads of different genotypes using the StepOnePlus real-time PCR system (Applied Biosystems). Each analysis was performed in three technical replicates in a total volume of 18 μl reaction mix containing 2 μl cDNA template, 10 μl 2× Sensimix SYBR and Fluorescent kit (QT615-05; Bioline), 2 μl RNase-free water, and 4 μl of 1 μM gene-specific forward/reverse primers (200 nM final concentration each). Cycling conditions for all primers were as follows: 95°C for 10 min (one cycle); 95°C for 15 sec, 59°C for 30 sec, 72°C for 30 sec (45 cycles); and 72°C for 5 min (one cycle). Threshold cycle (Ct) values were calculated using StepOne software (version 2.2.2; Applied Biosystems). The ΔCt values for genes expressed in germ cells and in Sertoli cells were calculated by using the germ cell-specific gene *Ddx4* or the Sertoli cell-specific gene *Sox9*, respectively, as internal controls. The sequences of primers used in this study can be found in Supplemental Table S1 (all the Supplemental Data are available online at www.biolreprod.org).

Labeling of Arteries and Veins

A previously described dye-enhanced technique [36] with modification to whole body circulation [37] was used. The vasculature was labeled in mice at P17. Briefly, animals were anesthetized with ketamine (100 mg/kg) and xylene (5 mg/kg). The left ventricle was cannulated retrograde and the animal was well-perfused with freshly made buffer composed of adenosine (1 mg/ml), paparverine (40 μg/ml), and heparin (25 mg/ml) in PBS to wash out the blood. The left cardiac ventricle was cannulated retrograde through the previous cannulation site and the BLUE dye (PU4ii; VasQtec) with adequate viscosity to avoid capillary filling (resin:2-butanone [1:1]) was slowly infused. The perfusion was stopped after a few seconds, when the BLUE dye reached the testes. The dye was allowed to solidify for 10 min, and then the whole mouse was stored in 10% formalin. Each sample was imaged 24 h later using a stereomicroscope.

Spectroscopic Measurements of Total Hemoglobin and Hemoglobin Saturation

Optical spectroscopy measurements to collect the diffuse reflectance spectra were made with a fiber optic probe coupled to a Skinskan (J.Y. Horiba) as previously described [38]. Mice at neonatal (P5–P15), pubertal (P16–P30), young (P31–P45), and adult (P90) stages were anesthetized with the open-drop exposure method using a mixture of 20% (v/v) isoflurane in propylene glycol. Both testes were exposed through a small abdominal incision, and optical spectroscopy measurements were made by placing the fiber optic probe in direct contact with the testes surface four times (two times on the middle and one at each extreme). The diffuse reflectance spectra (480 to 600 nm) measurement was acquired with a photomultiplier tube set to 340 V. The diffuse reflectance data were then processed using a Monte Carlo–based model of diffuse reflectance to extract the physiological information related to absorption and scattering properties of the tissue to estimate total hemoglobin (Hb), its concentration, and its saturation [39]. Calibration of the probe was carried out by normalizing the diffuse reflectance data wavelength by wavelength to a reflectance puck measurement (Labsphere, Inc.) made with the probe in flush contact.

Western Blot Analysis

Isolated seminiferous tubules from decapsulated P0 and P30 right and left testes of both genotypes were homogenized in RIPA buffer containing 25 mM Tris-HCl, pH 7.4, 150 mM NaCl, 1 mM ethylenediaminetetraacetic acid, 10 mg/ml phenylmethylsulfonyl fluoride, 1% NP-40, 0.5% Na-deoxycholate, 50 mM NaF, 0.2 mM NA_3VO_4, and 1× protease cocktail (Sigma) and then centrifuged for 10 min at $9300 \times g$. Protein was quantified by the bicinchoninic acid protein assay (BCA, Pierce), and 25 μg of protein was loaded in a 8% polyacrylamide gel (SDS–PAGE) under reducing and denaturing conditions and then transferred to a activated polyvinylidene fluoride membrane (Bio-Rad) at 300 mA for 1 h. Polyvinylidene fluoride membrane was blocked with 5% (w/v) nonfat milk and 0.1% Tween in TBS (50 mM Tris-HCl pH 7.4, 150 mM NaCl) and then incubated overnight at 4°C with anti-HIF-1α (NB-100-479, 1:1000 dilution; Novus Biological) or anti-β-actin (A-5060, 1:5000 dilution; Sigma). Membranes were then incubated with the secondary antibody goat-anti-rabbit-horseradish peroxidase-conjugated (111-036-003, 1:5000 dilution; Jackson ImmunoResearch) in blocking solution for 1 h at room temperature. Western blots were developed with ECL (Amersham) and exposed to film (Kodak).

Detection of Reactive Oxygen Species

To evaluate the intracellular levels of reactive oxygen species (ROS), we used the fluorescent indicator chloromethyl 2′,7′-dichlorodihydrofluorescein diacetate (CM-H2-DCF-DA) (Molecular Probes). Briefly, right and left testes at P14 were collected in Dulbecco-modified Eagle medium (DMEM, Thermo Fisher Scientific Inc.), and seminiferous tubules were dissociated by 5 min incubation in trypsin. The cellular suspension was rinsed and distributed to four tubes. One tube was used as a negative control for measuring cellular autofluorescence. The second group of cells was incubated with 1 μM DCF-DA for 10 min. The third tube was the positive control: cells were incubated first with 1 mM H_2O_2, a donor of ROS, for 10 min, washed once with Dulbecco-modified Eagle medium, and then incubated with 1 μM DCF-DA for 10 min. The last tube was used to evaluate cell viability by trypan blue (Sigma). After treatment, cells were fixed in 10% methanol for 10 min and washed in PBS. Total fluorescence of DCF was measured using flow cytometry within 3 h.

Nucleotide Measurements

For measurements of whole-cell AMP, ADP, ATP, NAD^+, and NADH, seven to eight right and left testes at P10 were pooled independently, snap-frozen, and stored at −80°C until three independent pools of 20 mg of tissue were collected. Tissue homogenates were prepared at 100 mg wet weight per ml extraction solvent. Briefly, a solution of methanol (6.7 μl/mg wet weight tissue) containing internal standards was added to each sample. The samples were then minced with scissors and homogenized using a hand-held homogenizer. Chilled water (3.3 μl/mg wet weight tissue) and then hexanes (10 μg/mg [w/w] tissue) were added to each sample, and the tubes were thoroughly mixed and centrifuged. The aqueous extract was then processed and nucleotide concentration analyzed by liquid chromatography tandem mass spectrometry (LC-MS/MS) according to previously reported methods [40, 41]. Concentrations were calculated based on the ratio of signal to the internal standards $^{13}C_{10}$-ATP, $^{13}C_{10}$,$^{15}N_5$-AMP, or nicotinamide 1,N6-ethenoadenine dinucleotide as appropriate. The AMP/ATP, ADP/ATP, NAD^+/NADH, and $NADP^+$/NADPH ratios were calculated for right and left testes and expressed as the fold change relative to the right testis for each genotype.

RESULTS

Spermatogenic Failure in Dnd1$^{Ter/+}$ 129/SvJ Mice Is Biased to the Left Testis

In our breeding pool, mice of the 129/SvJ background that carry a homozygous mutation in the RNA-binding protein *Dnd1* (*Dnd1*$^{Ter/Ter}$) show a 54% incidence of spermatogenic failure and 65% incidence of testicular teratoma with some mice showing both phenotypes in one testis. Heterozygous mutants on the same background (129/SvJ *Dnd1*$^{Ter/+}$) display a reduced incidence of both phenotypes. In a total of 490 *Dnd1*$^{Ter/+}$ mice analyzed between P0 and 6 mo of age, ~10% showed testicular atrophy compared to ~1% among 313 129/SvJ wild-type males. Testicular atrophy was usually evident as a clear reduction in the size of one testis compared to the other in ~10% *Dnd1*$^{Ter/+}$ adult males (Fig. 1a). In the *Dnd1*$^{Ter/+}$ mice that exhibited unilateral testicular atrophy, the incidence of the phenotype was strongly biased to the left testis (95%) compared to the right testis (5%).

To determine when the difference between right and left testes was first detectable, we performed a histological comparison of 129/SvJ *Dnd1*$^{+/+}$ and *Dnd1*$^{Ter/+}$ testes at multiple stages between P3 and P180. While many tubules showed normal progression of spermatogenesis, differences were first detected between the right and left testes at P15 (Fig. 1b). The tubule diameter was measured using FIJI software as the average of two perpendicular measurements in >300 tubules at each stage (shown are P15, P30, and P180) of each

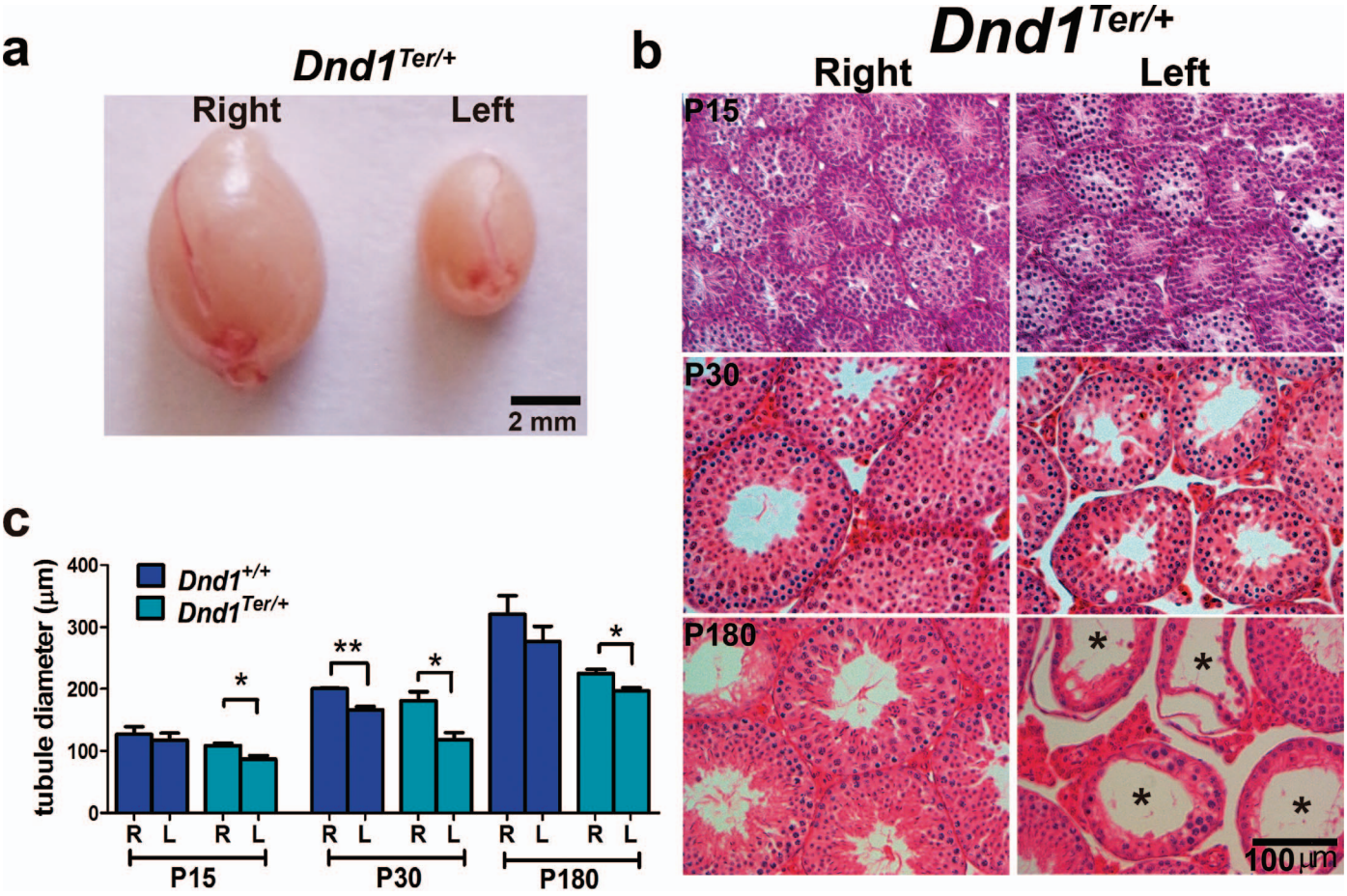

FIG. 1. Spermatogenic failure is biased to the left testis of 129/SvJ *Dnd1*$^{Ter/+}$ mice. **a**) An obvious size difference was frequently observed between right and left testes in adult 129/SvJ *Dnd1*$^{Ter/+}$ mice. **b**) Histological evaluation of 129/SvJ *Dnd1*$^{Ter/+}$ testis stained with hematoxylin and eosin showed a progressive disruption of spermatogenic development in the left testis beginning at P15 and abundant Sertoli cell-only tubules in the left testis by P180 (stars). **c**) Differences in tubule diameter, quantified through morphometric analysis, showed the first significant differences between right and left testes by P15 in *Dnd1*$^{Ter/+}$ mice. Note that wild-type 129/SvJ mice also showed a similar trend, significant only at P30. *$P \leq 0.05$, **$P \leq 0.01$ ($n \geq 50$).

genotype. A significant difference between right and left tubule diameter was evident in both wild type and *Dnd1*$^{Ter/+}$ at P30 and persisted as a significant difference in *Dnd1*$^{Ter/+}$ at later stages, with heterozygous mice showing significant differences between the right and left testes at all three stages (Fig. 1c).

Male Gonocytes Develop Similarly in the Right and Left Testes of Dnd1$^{Ter/+}$ *Mice*

The bias in testicular atrophy between the right and left testes first evident at P15 might initiate during embryonic development or in early postnatal life. One possible explanation for the left-sided bias in male germ cell depletion could be that primordial germ cells colonize the right and left gonads with different frequency. To investigate this possibility, we introduced *Oct4-EGFP* into the 129/SvJ *Dnd1*$^{Ter/+}$ genetic background to label germ cells and counted the number of germ cells (OCT4-EGFP+ cells) that colonize the right and left genital ridges. At E11.5, a similar number of germ cells is present in the right and left gonads of 129/SvJ wild type and *Dnd1*$^{Ter/+}$ heterozygotes (Fig. 2, a and b), indicating that similar numbers of germ cells migrate to the right and left gonads in *Dnd1*$^{Ter/+}$ and wild-type males. We detected no bias in colonization or early proliferative expansion of the gonocyte population in the right and left gonads.

Once male germ cells arrive in the developing gonad at E11.5, they respond to signals from the testicular somatic environment [10, 11, 42]. Upstream signals controlling male development of germ cells include FGF9 [43, 44] and result in the transient upregulation of *Nodal*, an important autocrine regulator of germ cell fate. Mice with compromised Nodal signaling showed a reduction in germ cell pluripotency and a tendency to differentiate prematurely [45–47]. The Nodal-signaling pathway is particularly interesting because it is expressed with a left bias during primitive streak development and plays a role during the establishment of left/right asymmetry of the body axis [48].

To investigate whether genes associated with the Nodal pathway showed a right- or left-sided bias in germ cells, we compared the level of expression of *Nodal*, its coreceptor *Cripto*, and two negative modulators of the pathway, *Lefty1* and *Lefty2*, between the right and left testes. Germ cells and somatic cells were separated by FACS of OCT4-EGFP+ cells from right and left gonads at E13.5 and E14.5 (Fig. 2, c–f). We detected expression of Nodal pathway genes only in germ cells with the highest expression of members of the Nodal pathway at E13.5 as previously reported [47]. At this time point, *Nodal, Cripto,* and *Lefty1* trended slightly higher in *Dnd1*$^{Ter/+}$ mice, and both *Nodal* and *Lefty2* showed slightly higher expression in the left testis. However, there was wide variation among samples, perhaps because of the steep spike in expression at

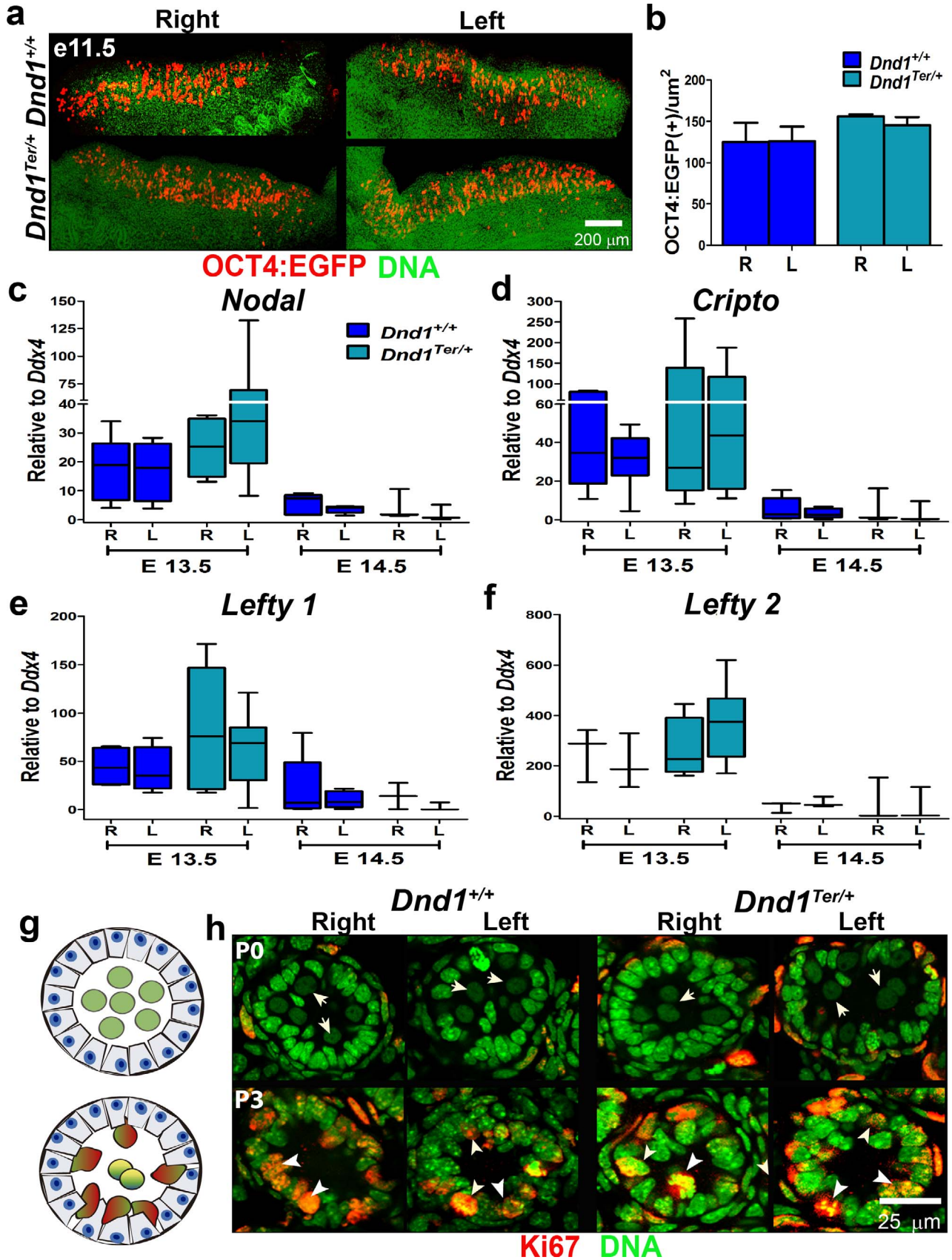

FIG. 2. Germ cells in the right and left testes of *Dnd1*$^{Ter/+}$ mice were similar to wild type during fetal and perinatal stages. **a**) Germ cells that arrived in the gonad were visualized and counted using the *Oct4-EGFP* reporter and confocal microscopy. **b**) Similar numbers of germ cells arrived in the right and left gonads by E11.5 in 129/SvJ *Dnd1*$^{+/+}$ and *Dnd1*$^{Ter/+}$ mice (n = 7 for each genotype). Expression of the autocrine regulators of germ cell development, *Nodal* (**c**), *Cripto* (**d**), *Lefty1* (**e**), and *Lefty2* (**f**) were quantified by qPCR in FACS OCT4-EGFP+ male germ cells at E13.5 and E14.5. Although there was a trend toward higher expression of this pathway in *Dnd1*$^{Ter/+}$ mutants, no significant differences were detected between the right and left testes (n ≥ 4).

E13.5, and none of these differences were significant. Expression of pathway genes rapidly declined by E14.5 in right and left gonads of both genotypes. These results suggest that Nodal signaling, which promotes male gonocyte survival, proliferation, and retention of pluripotency [47], may trend slightly higher in mutants than in wild type, but is not significantly different between the right and left testes of 129/SvJ *Dnd1*$^{+/+}$ or *Dnd1*$^{Ter/+}$ mice and is unlikely to explain the left-sided spermatogonial degeneration phenotype.

In the fetal testis, gonocytes are localized in the center of testicular cords, the precursors of the seminiferous tubules. Between E13.5 and E15.5, gonocytes enter mitotic arrest (G0) and remain quiescent until after birth [10, 13, 49]. To determine whether gonocytes progress through these differentiation steps normally in the right and left testes of 129/SvJ *Dnd1*$^{+/+}$ or *Dnd1*$^{Ter/+}$ mice, we used an antibody against Ki67, a marker expressed at all stages of the cell cycle except G0. At birth (P0), gonocytes, which are identified by their large, round, pale-staining nuclei (Fig. 2, g and h, top panel, arrows), were localized in the center of tubules in both the right and left testes of wild-type and *Dnd1*$^{Ter/+}$ mice. Based on the absence of Ki67 staining in these cells, we concluded that they had arrested normally in G0 of cell cycle. Soon after birth, male gonocytes resume their cell cycle and migrate to the basement membrane of the seminiferous tubules. In P3 testes of wild-type and *Dnd1*$^{Ter/+}$ genotypes, gonocytes had initiated this process and resumed expression of Ki67, indicating that they had exited cell cycle arrest (Fig. 2, g and h, bottom panel, arrowheads). In addition, we found no significant differences in the timing of testicular descent between the right and left testes (data not shown). In summary, we found no evidence of an abnormal spermatogonial differentiation program between the left and right testes in *Dnd1*$^{Ter/+}$ mice during fetal or perinatal stages.

Increased Apoptosis in the Left Testis of Dnd1$^{Ter/+}$ *Mice Explains the Decline in SSCs*

Based on the significant differences in tubule diameter detected between the right and left testes in both wild-type and *Dnd1*$^{Ter/+}$ mice, with heterozygous mice showing significant differences from P15 onward (Fig. 1c), we investigated whether apoptosis of SSCs was increased in the left testis. Costaining of P12-isolated testicular tubules for PLZF, a marker of SSCs, and active CASPASE-3, cPARP (Fig. 3a), or terminal deoxynucleotidyl transferase dUTP nick end labeling alone (Supplemental Fig. S1a), revealed a nearly 2-fold increase in apoptotic germ cells in the left testis at P12 (Fig. 3b).

To investigate the ongoing loss of spermatogonia, we used antibodies against PLZF and STRA8 (a marker of spermatogonial entry into meiosis used to identify tubules in the same stage of spermatogenesis). We quantified PLZF$^+$ spermatogonia at P17, P25, and P34 in whole isolated stage-matched tubules from wild-type and *Dnd1*$^{Ter/+}$ testes. At P17, the number of PLZF$^+$ and STRA8$^+$ cells was lower in heterozygous than in wild-type testes, but in both genotypes, the number was lower in the left compared to the right testis. There was a rapid decline in spermatogonial numbers between P17 and P25 in wild-type testes. By P25, the number of PLZF$^+$ cells in both genotypes was similar, but significantly lower in the left testes of *Dnd1*$^{Ter/+}$ mice. By P34, numbers of PLZF$^+$ cells stabilized in left and right testes of wild-type mice, but continued to decline in the left testis of *Dnd1*$^{Ter/+}$ mice (Fig. 3c). When we introduced a heterozygous mutation in *Bax*, a proapoptotic member of the Bcl-2 protein family, into the 129/SvJ *Dnd1*$^{Ter/+}$ background, we recovered wild-type numbers of SSCs based on PLZF immunofluorescence (Fig. 3d). Together these results indicate that the sidedness of spermatogenic failure in *Dnd1*$^{Ter/+}$ mice is due to early postnatal cell death resulting in a decrease in the population of PLZF$^+$ SSCs.

Apoptosis of SSCs in the Left Testis Is Not Associated with Obvious Defects in Sertoli Cells or Paracrine Signaling

In testes of prepubertal (P18-P20) *Dnd1*$^{Ter/+}$ mice, labeling with the spermatogonial marker GCNA (Fig. 4a) and the pachytene marker δH2AX (Fig. 4b) revealed elevated germ cell depletion in the left testis relative to the right. This was also observed in wild-type testes at this stage, although we did not detect empty tubules as seen in *Dnd1*$^{Ter/+}$ testes (Fig. 4a, asterisk). To determine whether the number and basic structure of Sertoli cells were normal, we used a nuclear marker of Sertoli cells, SOX9 (Fig. 4a), as well as a cytoplasmic marker, TUJ1 (Fig. 4b), which reveals the differentiated cytoplasmic structure of Sertoli cells. Neither of these markers revealed differences between the right and left testes. These results suggest that the asymmetry in testicular atrophy arises after birth and is independent of gross defects in Sertoli cells.

Several growth factors secreted by Sertoli cells modulate spermatogonial development through paracrine signaling [50]. We investigated whether the expression of a group of well-characterized growth factors produced by Sertoli cells, *Cxcl12, Gdnf, KitL* (SCF), and *Fasl,* or their germ cell receptors*, Cxcr4, Gfrα1, Kit,* and *Fas,* differed between the right and left testes at a stage prior to the first evidence of germ cell loss in the left testis. *Cxcl12* and *Gdnf* growth factors and their receptors, *Cxcr4* and *Gfrα1*/*Ret,* are associated with the stimulation of SSC self-renewal [17, 18]; the expression of *Kit* and its receptor *KitL* (also known as *SCF*) are associated with the first wave of mitotic, differentiating spermatogonia [51]; and expression of the dead receptor *Fas* and its ligand *FasL* limits the number of germ cells by regulating the activation of the extrinsic pathway of apoptosis [20, 52].

To evaluate the expression of these paracrine factors, we isolated right and left testes tubules of wild-type and *Dnd1*$^{Ter/+}$ males at P8 (5 days prior to the time when spermatogonial loss is evident), and compared expression levels by qPCR (Fig. 4, c–j). The results were normalized to levels of *Sox9* in the case of genes expressed in Sertoli cells (Fig. 4, c, e, g, and i) and to levels of *Ddx4* in the case of genes expressed in spermatogonia (Fig. 4, d, f, h, and j). Based on MVH/DDX4 staining, the number of germ cells did not show differences between right and left testes at P8 (Supplemental Fig. S2a). The expression levels of *Cxcl12* and *Gdnf* growth factors and their receptors, *Cxcr4* and *Gfrα1* (Fig. 4, c–f), as well as *Ret* (Supplemental Fig. S2b), were similar in right and left testes of both genotypes. In *Dnd1*$^{Ter/+}$ testes, the expression of *Kit and KitL* did trend higher in the right testis (Fig. 4, g and h), but staining for KIT did not reveal differences between the right and left testes (Supplemental Fig. S2c). The expression of *Fas* and *FasL* was very low in all cases (Fig. 4, i and j). Although the

g and **h**) Similar to wild type, at P0 (top panel), gonocytes with large pale nuclei were localized in the center of the seminiferous tubules and were negative for Ki67 (arrow). By P3 (bottom panel), gonocytes of both genotypes showed normal migration to the basement membrane of the tubules and resumed proliferation based on expression of Ki67 (arrowhead) (n = 6 for each genotype).

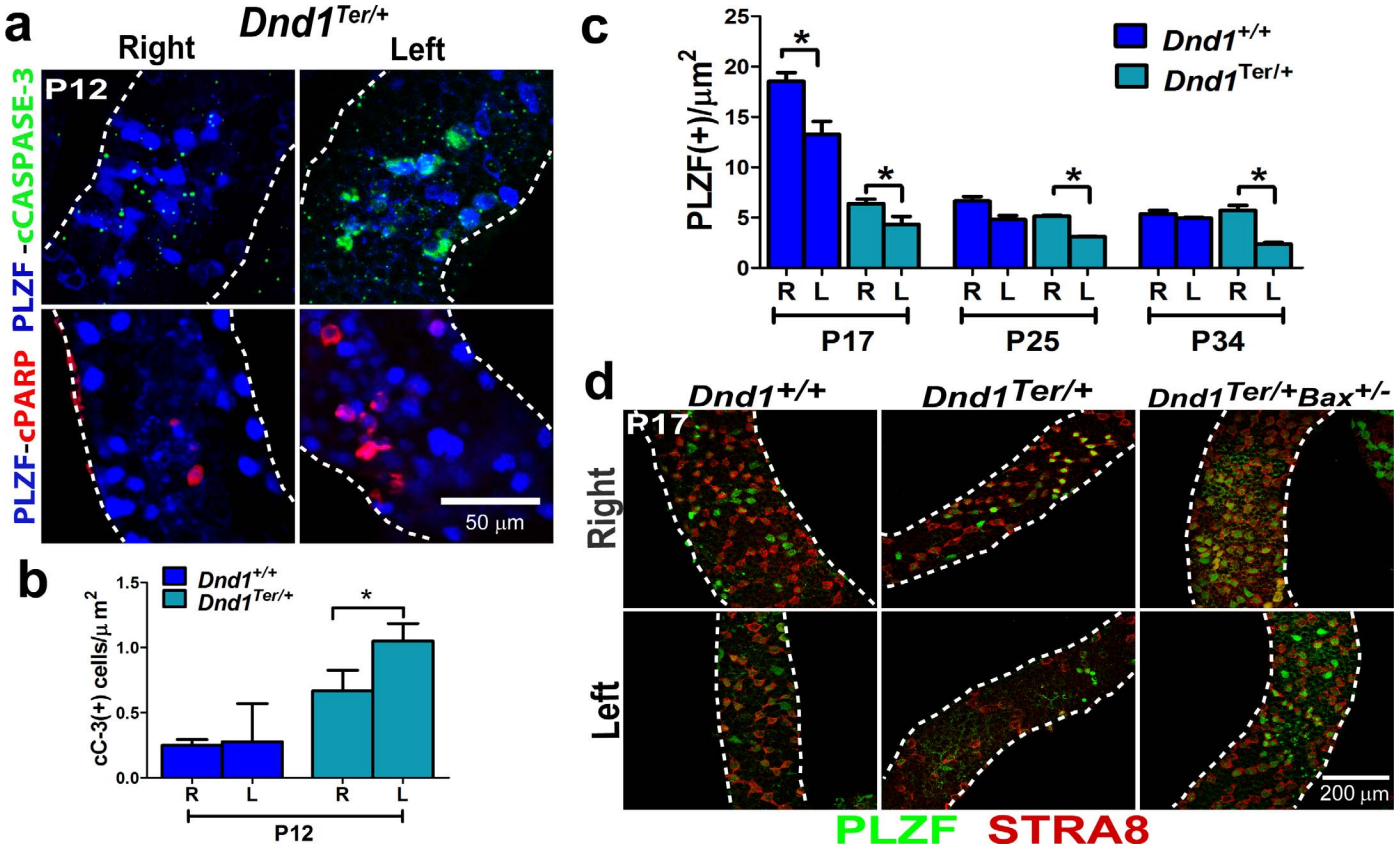

FIG. 3. The reduced number SSCs in the left testis of *Dnd1*$^{Ter/+}$ mice is due to apoptosis. **a**) Immunofluorescence of whole-mount tubules of *Dnd1*$^{Ter/+}$ testes at P12. In tubules from the left testis, more SSCs (PLZF^{+} cells) were positive for cCASPASE-3 (green, top panel) and cPARP (red, bottom panel) (n = 6 mice of each genotype). **b**) Quantification of the numbers of activated CASPASE-3 (cC-3)-positive cells in the right and left testes of both genotypes showed that apoptosis is more frequent in *Dnd1*$^{Ter/+}$ compared to wild-type mice (n = 10 of each genotype, $*P \leq 0.05$). **c**) Fewer PLZF^{+} cells were detected in *Dnd1*$^{Ter/+}$ mice by P17 compared to wild-type mice. By P25, the numbers of PLZF^{+} cells in the right testis of wild-type and *Dnd1*$^{Ter/+}$ mice were similar. However, the number of PLZF^{+} cells continued to show a significant decline in the left testis of *Dnd1*$^{Ter/+}$ at P34 (n = 6 mice of each genotype, at each stage, $*P \leq 0.05$). **d**) Immunofluorescence and confocal microscopy using antibodies against PLZF (green) and STRA8 (red), a marker of cells undergoing meiosis (used to select tubules in the same stage of spermatogenesis), revealed the reduction of SSCs and differentiating spermatogonia in the left testis of both genotypes. This difference was more severe in *Dnd1*$^{Ter/+}$ heterozygous mutants. The introduction of a single mutant allele of the proapoptotic gene *Bax* rescued the number of spermatogonia in the left testis (n = 6 mice of each genotype).

variance between samples was high, no consistent differences were observed for any of these growth factors. These results suggest that altered expression of well-characterized paracrine-signaling pathways involved in SSC self-renewal, differentiation, and survival during the early postnatal period are unlikely to explain the asymmetric spermatogenic loss phenotype.

The Origin of the Left and Right Spermatic Arteries Is Asymmetric in 129/SvJ Mice

The vascular system that irrigates and drains the testis in mice is highly variable among inbred strains [53]. In 1982, Leroy Stevens made the observation that in his colony of 129/Sv mice, the origin of the right spermatic artery was superior to that of the left. Stevens crossed the situs inversus viscerum gene onto the 129/Sv strain and found that the sidedness of testicular phenotypes reversed from the left to the right in animals in which the body axis was reversed [34]. Because we found no evidence that body axis asymmetry molecular pathways differ in the left and right testes (Fig. 2, c–f), we considered the possibility that physiological differences between the right and left testes that arise due to differences in vascular architecture might be responsible for the difference in SSCs viability between the right and left testes.

Significant variation in the anatomical structure of the spermatic arteries and veins has been reported among inbred strains [53]. To determine whether a difference in the origin of the right and left testicular artery in our 129/SvJ colony was consistent with Stevens' report [34], we perfused the arterial system with BLUE dye by injection into the left ventricle of four wild-type and four heterozygous mice. This procedure labeled all the arteries and veins within seconds. Consistent with Stevens' observations, the origin of the right spermatic artery was superior to the origin of the left spermatic artery in 129/SvJ mice of both wild-type and heterozygous genotypes (Fig. 5, a and b), and we found this left/right difference in arterial architecture consistently present from E16.5 onward (Supplemental Fig. S3).

The differences in vascular architecture, which may also include differences in the venous structure, could differentially affect blood flow, oxygen supply, or ROS in the left and right testes leading to a reduction in the number of SSCs evident by P15. To compare blood flow and oxygen availability in the right and left testes, we used a quantitative method of diffuse reflectance spectroscopy in the visible spectrum [38, 39]. We measured the level of total Hb, as a reflection of the rate of blood flow, and the saturation of Hb, as a proxy for oxygen availability, in the right and left testes of 129/SvJ wild-type and *Dnd1*$^{Ter/+}$ mice. The concentration of total Hb (~25 μM) was

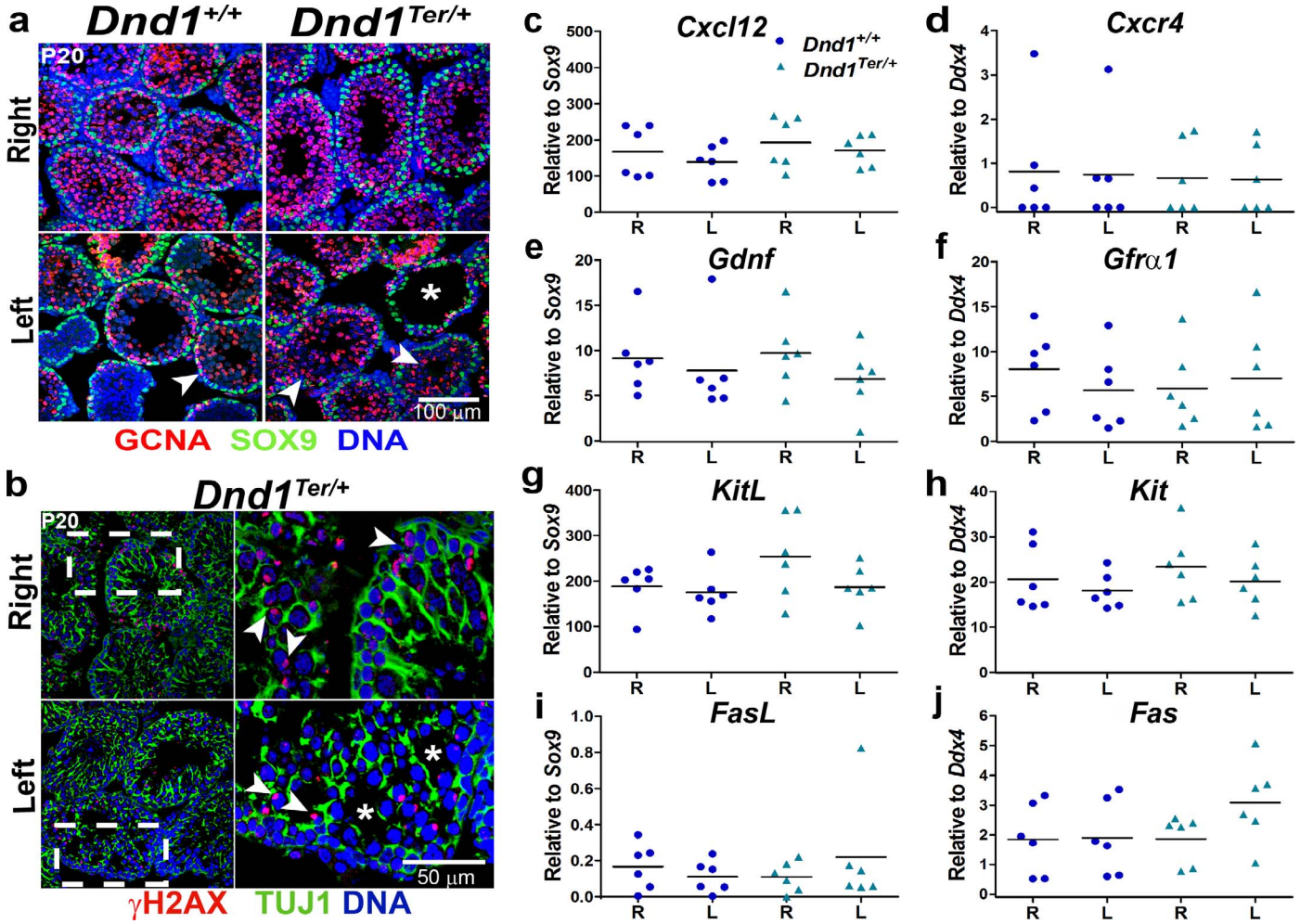

FIG. 4. The number and distribution of Sertoli cells and the expression of important paracrine signals were indistinguishable from wild type in the right and left testes. The number of Sertoli cells, stained with SOX9 (**a**) as well as (**b**) the distribution of Sertoli cell cytoplasm from the basement membrane to the lumen of the tubule, based on TUJ1 staining, was normal at P20. The frames to the right in **b** are higher magnification images of the box defined by the broken line in the left-most frames. However, spermatogonia (GCNA+, arrowhead in **a**, and γH2AX+, arrowhead in **b**) were reduced in some tubules (**a** and **b**, asterisk) in the left testis of heterozygous mice (n = 6 mice of each genotype). Expression of a group of growth factors produced by Sertoli cells—(**c**) *Cxcl12,* (**e**) *Gdnf,* (**g**) *KitL* (SCF), and (**i**) *Fasl*—and their receptors expressed by germ cells—(**d**) *Cxcr4,* (**f**) *Gfrα,* (**h**) *Kit,* and (**j**) *Fas*—were evaluated by qPCR in whole tubules at P8. Sertoli-expressed genes were normalized to *Sox9,* whereas germ cell-expressed genes were normalized to *Ddx4.* No significant differences were detected (n = 6 mice of each genotype).

not significantly different among samples of right and left testes in either genotype (Fig. 5c). However, Hb saturation was consistently lower in the left testis of both genotypes at all stages (the single exception is a higher value in the left testis of wild-type mice at P16–P30). The difference in Hb saturation was only statistically significant in wild-type mice at P5–P15 (65% in the right testis vs. 52% in the left testis), although a similar difference was measured in *Dnd1*$^{Ter/+}$ (61% in the right testis vs. 45% in left testis). The saturation of Hb, and therefore oxygen availability, was consistently lower in the left testis during the stage when increased apoptosis of spermatogonia was detected. In contrast, evaluation of ROS production, by measuring the percentage of DCF-positive cells (see *Materials and Methods*), showed no difference between the right and left testes (Supplemental Fig. S4a).

The cellular response to a decrease in oxygen tension is in part mediated by the stabilization of the transcription factor hypoxia inducible factor-1 alpha (HIF-1α) that activates the transcription of genes related to differentiation, metabolism, and survival [54, 55]. To determine whether lower oxygen availability was correlated with differences in levels of HIF-1α, we collected individual right and left testes from *Dnd1*$^{+/+}$ and *Dnd1*$^{Ter/+}$ genotypes at P0 and P30, isolated protein, and analyzed HIF-1α levels by Western blot analysis (Fig. 5, e and f). In both wild-type and *Dnd1*$^{Ter/+}$ genotypes, HIF-1α was stabilized in the left testis relative to the right. These results are consistent with our findings that the availability of oxygen in the left testis is lower relative to the right testis.

Metabolic Differences Between Left and Right Testes Could Lead to Apoptosis of SSCs

The levels of metabolites play a pivotal role in dictating whether a cell proliferates, differentiates, or remains quiescent [56]. The levels of nucleotides (AMP, ADP, and ATP) and the oxidized and reduced forms of nicotinamide adenine dinucleotide (NAD^+, $NADP^+$, NADH, and NADPH) reflect the metabolic health and redox state of the tissue [57–59]. We hypothesized that due to lower oxygen availability, the ability of the left testis to produce energy was compromised. To test this hypothesis, we pooled seven to eight right and left whole testes of wild-type and *Dnd1*$^{Ter/+}$ mice at P10 and measured

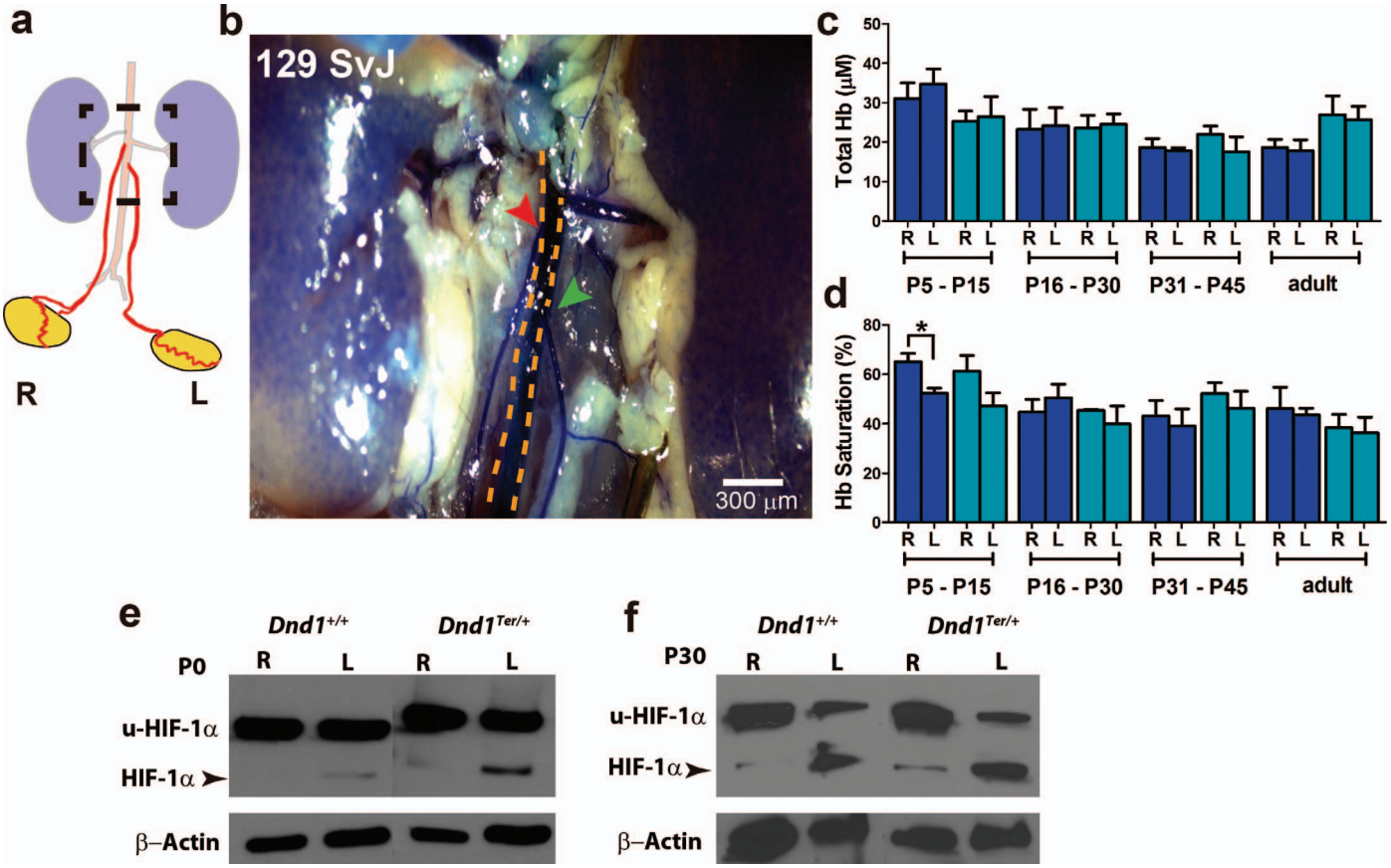

FIG. 5. Differences in vascular architecture between the right and left testes are correlated with oxygen availability. BLUE dye was injected through the heart of P17 *Dnd1* wild-type and heterozygous mice, labeling their vascular systems. **a**) Schematic representation of the origin of right and left spermatic arteries from the aorta, illustrating the superior divergence of the right. The boxed region of this diagram is photographed in **b**. In 129/SvJ mice, the right spermatic artery (red arrowhead) branches from the aorta (yellow dashed line) superior to the left (green arrowhead) (n = 8 mice of each genotype). Using spectroscopic methods, (**c**) total Hb and (**d**) Hb saturation were measured in right and left testes at P5–P15, P16–P30, P31–P45, and adult. Significant differences in the percentage of Hb saturation were detected between right and left testes at P5–P15 (n = 6 mice at each stage of each genotype, $*P \leq 0.05$). Higher levels of HIF-1α (arrowhead) were detected by Western blot analysis in the left testis compared to the right testis of wild-type and $Dnd1^{Ter}$ mice at (**e**) P0 and (**f**) P30; u-HIF-1α: ubiquitinated HIF-1α (n = three independent Western blots).

the levels of ATP, ADP, AMP, NAD^+, NADH, $NADP^+$, and NADPH using LC-MS/MS (Fig. 6). Based on three biological replicates, the levels of AMP (Fig. 6a) trend similarly in the right and left testes of wild-type mice (97.3 and 104.3 pmol/mg tissue, respectively) whereas, in $Dnd1^{Ter/+}$ mice, the levels of AMP trended higher in the left testis compared to the right (98.1 pmol/mg tissue in the right and 148.7 pmol/mg tissue in the left testis). No differences in the levels of ADP or ATP were detected between right and left testes of wild-type mice (2211.4 in the right testis vs. 2176.7 pmol/mg tissue in the left testis for ATP). However, in $Dnd1^{Ter/+}$ mice, the levels of ADP trended higher in the left testis (553.6 pmol/mg tissue) compared to the right testis (313.6 pmol/mg tissue), and the levels of ATP trended lower in the left testis (1808.7 pmol/mg tissue) compared to the right (2607.5 pmol/mg tissue). These differences resulted in an increase in the fold change of the AMP/ATP (Fig. 6b) and ADP/ATP ratios (Fig. 6c) in the left testis relative to the right testis of $Dnd1^{Ter/+}$ mice.

The ratios of NAD^+/NADH and $NADP^+$/NADPH affect the activity of many enzymes involved in metabolic pathways, oxidative stress, and mitochondrial functions, and play an important role in regulating cell death [59]. The levels of NAD^+, NADH (Fig. 6d), and NADPH (Supplemental Fig. S4b) were lower in the left testis than the right in $Dnd1^{Ter/+}$ mice (Fig. 6d). The NAD^+/NADH (Fig. 6e) and NADP+/NADPH (Supplemental Fig. S4c) ratios were similar between right and left testes of wild-type mice, but these ratios were higher in the left testis relative to the right in $Dnd1^{Ter/+}$ mice (Fig. 6e). These results reveal important metabolic differences between the right and left testes of $Dnd1^{Ter/+}$ mice that precede testicular atrophy and suggest compromised homeostasis in the left testis.

DISCUSSION

In 1954, Leroy Stevens reported that 1% of 129/SvJ males develop testicular teratomas, 5% undergo spermatogenic failure, and that both of these phenotypes show a strong bias to the left side [25]. Stevens showed that crossing the situs inversus viscerum mutation onto the 129/SvJ strain led to reversal of this bias to the right testis in accordance with the reversal of the internal organs [34]. During Stevens breeding experiments, a spontaneous mutation arose (*Ter*) that increased the incidence of these phenotypes [22]. In 2005, this mutation was mapped to the gene encoding the RNA-binding protein, *Dnd1* [26]. In our colony, $Dnd1^{Ter/Ter}$ mutants mice show a >60% incidence of teratomas and/or spermatogenic failure that is usually bilateral. However, $Dnd1^{Ter/+}$ heterozygotes show a 10% incidence of spermatogenic failure, and 95% of the unilateral cases occur in the left testis, suggesting that heterozygous mutants are sensitized to

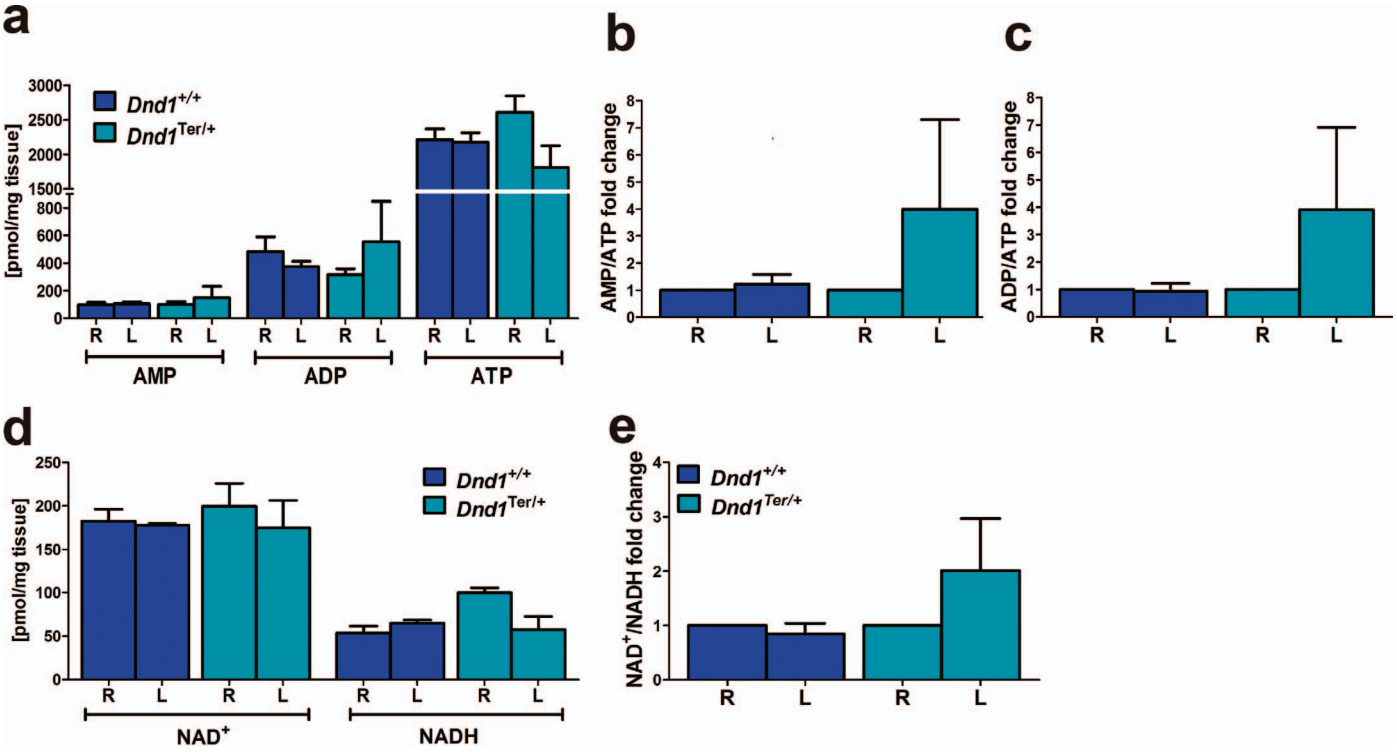

FIG. 6. Differences in the levels of AMP, ADP, ATP, NAD^+, and NADH between right and left testes. Right and left testes from seven to eight wild-type and *Dnd1*$^{Ter/+}$ mice at stage P10 were collected and independently pooled (n = 3 biological replicates for right and left testes of each genotype). **a**) Tissue homogenates were analyzed using LC-MS/MS to measure the levels of AMP, ADP, and ATP, and the (**b**) AMP/ATP and (**c**) ADP/ATP ratios were calculated and expressed, for each genotype, as the fold change relative to the right testis. B) Levels of NAD+ and NADH were measured in the same samples and (**e**) NAD^+/NADH ratios were calculated and expressed, for each genotype, as the fold change relative to the right testis.

subtle molecular or physiological differences between the right and left testicular microenvironment that could represent novel influences on the process of spermatogonial survival and development.

We began investigating the cause of this curious phenotype by determining when the first signs of germ cell loss were detected. The numbers of germ cells colonizing the left and right testes were similar at fetal stages. We found that differences were first visible at P15, when testicular tubules were smaller in the left than in the right testis (Fig. 1b), suggesting that molecular or environmental signals affecting germ cell development differ between the left and right testes during this developmental window. One possibility was that the molecular pathways that control the establishment of left/right body axis asymmetry (*Nodal*, *Cripto*, *Lefty1*, and *Lefty2*) were expressed at different levels in germ cells populating the right and left gonad. However, we found no significant differences in the expression of these genes in germ cells from right and left testes in wild-type mice, which would be expected given that 129/SvJ wild-type mice show a left/right bias. There was significant variation among our samples that could be related to interplay between the exact timing of the dissection and the rapid spike in *Nodal* expression at E13.5. Variation was more extensive in heterozygotes, and especially in the left testis. Because *Nodal* overexpression is associated with many tumors [60, 61], this may reflect the presence of unstable SSCs in the sample susceptible to initiating degeneration or tumor formation. However, elevation of Nodal would be expected to be associated with improved survival of germ cells [47]; thus, left/right differences in the Nodal-signaling pathway in germ cells do not appear to be the initiating cause of the asymmetry of the degeneration phenotype.

Just after birth, we found that germ cells migrate to the periphery of the seminiferous tubules in the right and left testes and resume mitosis normally in heterozygous mutants. Consistent with this result, no differences in levels of MVH were evident at an early postnatal stage (P8), suggesting that germ cell loss begins between P8 and P15. Cell death, as measured by cCASPASE3, cPARP, and terminal deoxynucleotidyl transferase dUTP nick end labeling, all indicated elevation of apoptosis in the left versus the right testis between P12 and P14. The number and structure of Sertoli cells were similar in the left versus the right testis as well as the expression levels of paracrine signals produced by Sertoli cells to regulate germ cell survival and proliferation, but the variation among samples was again high. The low expression of Fas and FasL, which activate the extrinsic pathway of apoptosis [62], suggest that apoptosis of germ cells is instead triggered by the intrinsic pathway initiated within the cell in response to DNA damage, loss of survival factors, or cellular stress [62].

Based on the observation that the degeneration phenotype could be reversed to the right testis after introduction of the situs inversus viscerum mutation [34], we hypothesized that germ cells in 129/SvJ mice are sensitized to physiological differences in the testicular microenvironment. We used a variety of techniques to explore this possibility. We showed that in 129/SvJ mice the origin of the left spermatic artery is superior to the origin of the right spermatic artery (Fig. 5a). Although the levels of total Hb were similar between right and left testes, Hb saturation was different in both wild-type and heterozygous mice between the ages of P5–P15, the developmental window when elevated apoptosis of SSCs occurs. Aging decreases the microvascular levels of oxygen in rat

testes [63], which might explain why the differences in Hb saturation did not increase in older mice. Future experiments to support our findings might include differential measurements of interstitial and microvascular oxygen levels as well as quantification of the local oxygen delivery-to-oxygen uptake relationship. Although differences in the left and right testes of wild-type and heterozygous mice were similar, greater variation in heterozygotes prevented a calculation of significance. Given the 10% incidence of spermatogenic failure, it seems likely that there are outliers in the population reflected in this data.

In both wild type and heterozygous mutants, HIF-1α was upregulated in the left testis, although this effect was more pronounced in mutants suggesting that the differences in Hb saturation has physiological consequences. This is consistent with Stevens' original finding that the asymmetric degeneration phenotype occurs in wild-type 129/SvJ mice, albeit at a 10-fold lower frequency. Overall, our results indicate that anatomical differences in vascular architecture between the right and left testes are associated with differences in the availability of oxygen, which may affect the energetic and redox state, compromising the environment for the survival of SSCs. However, levels of HIF-1α can also be regulated by insulin [64], IGF [65], and possibly other metabolites. Therefore, we cannot eliminate the possibility that metabolic differences between the left and right testes play a role in stabilizing HIF-1α.

The effects of low oxygen tension (hypoxia) depend on the context in which it occurs. For example, in hematopoietic, mesenchymal, and neural stem cell niches, hypoxia maintains the undifferentiated state, promoting self-renewal and anaerobic metabolism [66, 67]. On the other hand, hypoxia induces cell death via apoptosis in the brain [68]. In the testis, hypobaric hypoxia can induce spermatogenic failure by inducing the apoptosis of spermatogonia and spermatocytes [69] and can also affect testicular metabolism [70]. Our metabolic analyses comparing the left and right testes using LS-MS/MS showed that AMP/ATP and ADP/ATP ratios were elevated in the left testis relative to the right just prior to the stage when extensive cell death occurs. However, this difference was only detectable in *Dnd1* heterozygotes. Because hypoxia and HIF-1α upregulation are common to both mutant and wild-type left testes, the elevation of AMP/ATP and ADP/ATP ratios might result from independent or additional effects of loss of a single allele of *Dnd1*. Alternatively higher HIF-1α in heterozygous mutants may meet a threshold that triggers other metabolic changes. High AMP/ATP and ADP/ATP ratios have been described in cells susceptible to cell death [57, 58]. In future experiments, it would be interesting to determine whether a decline in ATP, caused by hypoxia, with the concomitant increases in AMP/ATP ratio, is sensed by AMP-dependent protein kinase (AMPK). The activation of AMPK inhibits mTORC1, reducing cell growth and proliferation [71]. This can lead to the phosphorylation and activation of mitogen-activated protein kinase p38, which causes the translocation of cytosolic Bax to the mitochondria and triggers apoptosis [58]. AMPK also upregulates glucose uptake and activates glycolytic enzymes [72], stimulating glycolytic production of ATP and thus maintaining a sufficient ATP level for the execution of apoptosis.

In addition to differences in AMP/ATP and ADP/ATP ratios, the left testis also had higher $NAD(P)^+$/NAD(P)H ratios relative to the right. Under conditions of cellular stress, the DNA damage repair enzyme PARP is hyperactivated, which can induce the depletion of its substrate NAD^+ and intracellular ATP stores. This leads to the release of apoptosis-inducing factors and consequent cell death due to energy restriction [73]. The measurement of these metabolites in this study was limited to extracts from the whole right and left testes, without information about compartmentalization of pathways or cell types. Thus, the intercellular and subcellular metabolism in the SSC cell niche in vivo awaits further exploration. Interestingly, a left bias also has been described for testicular tumor incidence in humans [74, 75], and spermatogenic failure as a result of cryptorchidism and varicocele affect the left testis in the majority of the cases [76–78].

The capacity of SSCs to both produce differentiating spermatogonia and maintain their population through self-renewal is crucial to the maintenance of testicular homeostasis and spermatogenesis throughout reproductive life. One goal of studying the causes of spermatogenic failure is to find possible therapeutic targets to develop successful preventions and treatments. Recent studies have led to an increased understanding of how metabolic pathways may affect stem cell proliferation, homeostasis, and quiescence [67]. Our data suggests that the viability of SSCs also depends on the physiological microenvironment and that heterozygosity for the $Dnd1^{Ter}$ mutation renders carriers highly sensitive to environmental influences, perhaps offering a means of screening for other subtle factors that influence SSC fate. The differences in oxygen and metabolites that we have measured between the right and left testes may be reflective of many other differences that $Dnd1^{Ter/+}$ gonocytes can sense.

ACKNOWLEDGMENT

We thank Matt Cook for keeping initial statistical records reporting the right/left bias of the spermatogenic failure phenotype in our colony of 129/SvJ mice; Lindsey Seldin who, along with Cook, measured testicular descent in 129/SvJ mice; Pei-Lun Chu for his help labeling the vascular architecture; Tabitha Martin and Olga Ilkayeva (Stedman Center) for their help in preparing samples used for metabolomics analysis; and Gregory Palmer (Duke University) for facilitating the experiments measuring total Hb and its saturation. We thank Dr. Sally Kornbluth (Duke University) for kindly providing the antibody anti-HIF1α; Dr. Cagla Eroglu (Duke University) for kindly providing the antibody anti-TUJ1; and Dr. Michael D. Griswold (Washington State University) for providing the anti-STRA8 antibody. We thank Dr. Danielle Maatouk (Northwestern University) for her comments on this manuscript. We are also very appreciative of our funding from the Lalor Foundation and Comisión Nacional de Investigación Científica y Tecnológica (CONICYT) Chile, to X.B.M., as well as from NIGMS to B.C. for the laboratory's work.

REFERENCES

1. De Kretser DM, Baker HWG. Infertility in men: recent advances and continuing controversies. J Clin Endocrinol Metab 1999; 84:3443–3450.
2. Louis JF, Thoma ME, Sørensen DN, McLain AC, King RB, Sundaram R, Keiding N, Buck Louis GM. The prevalence of couple infertility in the United States from a male perspective: evidence from a nationally representative sample. Andrology 2013; 1:741–748.
3. Berookhim BM, Schlegel PN. Azoospermia due to spermatogenic failure. Urol Clin N Am 2014; 41:97–113.
4. Krausz C. Male infertility: pathogenesis and clinical diagnosis. Best Pract Res Clin Endocrinol Metab 2011; 25:271–285.
5. Ginsburg M, Snow MH, McLaren A. Primordial germ cells in the mouse embryo during gastrulation. Development 1990; 110:521–528.
6. Lawson KA, Hage WJ. Clonal analysis of the origin of primordial germ cells in the mouse. Ciba Found Symp 1994; 182:68–84.
7. Saitou M, Barton SC, Surani MA. A molecular programme for the specification of germ cell fate in mice. Nature 2002; 418:293–300.
8. Gomperts M, Garcia-Castro M, Wylie C, Heasman J. Interactions between primordial germ cells play a role in their migration in mouse embryos. Development 1994; 120:135–141.
9. Molyneaux K, Wylie C. The genome and the germ cell. Genome Biol 2002; 4:303.

10. McLaren A. Meiosis and differentiation of mouse germ cells. Symp Soc Exp Biol 1984; 38:7–23.
11. Feng C-W, Bowles J, Koopman P. Control of mammalian germ cell entry into meiosis. Mol Cell Endocrinol 2014; 382:488–497.
12. Hajkova P, Ancelin K, Waldmann T, Lacoste N, Lange UC, Cesari F, Lee C, Almouzni G, Schneider R, Surani MA. Chromatin dynamics during epigenetic reprogramming in the mouse germ line. Nature 2008; 452: 877–881.
13. Western PS, Miles DC, van den Bergen JA, Burton M, Sinclair AH. Dynamic regulation of mitotic arrest in fetal male germ cells. Stem Cells 2008; 26:339–347.
14. Bustamante-Marin X, Garness JA, Capel B. Testicular teratomas: an intersection of pluripotency, differentiation and cancer biology. Int J Dev Biol 2013; 57:201–210.
15. Yoshida S, Sukeno M, Nakagawa T, Ohbo K, Nagamatsu G, Suda T, Nabeshima Y. The first round of mouse spermatogenesis is a distinctive program that lacks the self-renewing spermatogonia stage. Development 2006; 133:1495–1505.
16. Matzuk MM, Lamb DJ. The biology of infertility: research advances and clinical challenges. Nat Med 2008; 14:1197–1213.
17. Yang Q-E, Kim D, Kaucher A, Oatley MJ, Oatley JM. CXCL12-CXCR4 signaling is required for the maintenance of mouse spermatogonial stem cells. J Cell Sci 2013; 126:1009–1020.
18. Jijiwa M, Kawai K, Fukihara J, Nakamura A, Hasegawa M, Suzuki C, Sato T, Enomoto A, Asai N, Murakumo Y, Takahashi M. GDNF-mediated signaling via RET tyrosine 1062 is essential for maintenance of spermatogonial stem cells. Genes Cells 2008; 13:365–374.
19. Packer AI, Besmer P, Bachvarova RF. Kit ligand mediates survival of type A spermatogonia and dividing spermatocytes in postnatal mouse testes. Mol Reprod Dev 1995; 42:303–310.
20. Lizama C, Alfaro I, Reyes J, Moreno R. Up-regulation of CD95 (Apo-1/Fas) is associated with spermatocyte apoptosis during the first round of spermatogenesis in the rat. Apoptosis 2007; 12:499–512.
21. Russell LD, Chiarini-Garcia H, Korsmeyer SJ, Knudson CM. Bax-dependent spermatogonia apoptosis is required for testicular development and spermatogenesis. Biol Reprod 2002; 66:950–958.
22. Stevens LC. A new inbred subline of mice (129-terSv) with a high incidence of spontaneous congenital testicular teratomas. J Natl Cancer Inst 1973; 50:235–242.
23. Sakurai T, Iguchi T, Moriwaki K, Noguchi M. The ter mutation first causes primordial germ cell deficiency in ter/ter mouse embryos at 8 days of gestation. Dev Growth Differ 1995; 37:293–302.
24. Cook MS, Coveney D, Batchvarov I, Nadeau JH, Capel B. BAX-mediated cell death affects early germ cell loss and incidence of testicular teratomas in Dnd1(Ter/Ter) mice. Dev Biol 2009; 328:377–383.
25. Stevens LC, Little CC. Spontaneous testicular teratomas in an inbred strain of mice. Proc Natl Acad Sci U S A 1954; 40:1080–1087.
26. Youngren KK, Coveney D, Peng X, Bhattacharya C, Schmidt LS, Nickerson ML, Lamb BT, Deng JM, Behringer RR, Capel B, Rubin EM, Nadeau JH, et al. The Ter mutation in the dead end gene causes germ cell loss and testicular germ cell tumours. Nature 2005; 435:360–364.
27. Asada Y, Varnum DS, Frankel WN, Nadeau JH. A mutation in the Ter gene causing increased susceptibility to testicular teratomas maps to mouse chromosome 18. Nat Genet 1994; 6:363–368.
28. Bhandari A, Gordon W, Dizon D, Hopkin AS, Gordon E, Yu Z, Andersen B. The Grainyhead transcription factor Grhl3/Get1, suppresses miR-21 expression and tumorigenesis in skin: modulation of the miR-21 target MSH2 by RNA-binding protein DND1. Oncogene 2013; 32:1497–1507.
29. Zechel JL, Doerner SK, Lager A, Tesar PJ, Heaney JD, Nadeau JH. Contrasting effects of Deadend1 (Dnd1) gain and loss of function mutations on allelic inheritance, testicular cancer, and intestinal polyposis. BMC Genet 2013; 14:54.
30. Weidinger G, Stebler J, Slanchev K, Dumstrei K, Wise C, Lovell-Badge R, Thisse C, Thisse B, Raz E. dead end, a novel vertebrate germ plasm component, is required for zebrafish primordial germ cell migration and survival.Curr Biol 2003; 13:1429–1434.
31. Suzuki A, Niimi Y, Saga Y. Interaction of NANOS2 and NANOS3 with different components of the CNOT complex may contribute to the functional differences in mouse male germ cells. Biol Open 2014; 3: 1207–1216.
32. Kedde M, Strasser MJ, Boldajipour B, Oude Vrielink JA, Slanchev K, le Sage C, Nagel R, Voorhoeve PM, van Duijse J, Orom UA, Lund AH, Perrakis A, et al. RNA-binding protein Dnd1 inhibits microRNA access to target mRNA. Cell 2007; 131:1273–1286.
33. Cook MS, Munger SC, Nadeau JH, Capel B. Regulation of male germ cell cycle arrest and differentiation by DND1 is modulated by genetic background. Development 2011; 138:23–32.
34. Stevens LC. Genetic influences on teratocarcinogenesis in mice. In: Tsukada Y (ed.), Genetic Approaches to Developmental Neurobiology, vol. 1. Tokyo: University of Tokyo; 1982:87–94.
35. Jameson SA, Natarajan A, Cool J, DeFalco T, Maatouk DM, Mork L, Munger SC, Capel B. Temporal transcriptional profiling of somatic and germ cells reveals biased lineage priming of sexual fate in the fetal mouse gonad. PLoS Genet 2012; 8:e1002575.
36. Zhang H, Prabhakar P, Sealock R, Faber JE. Wide genetic variation in the native pial collateral circulation is a major determinant of variation in severity of stroke. J Cereb Blood Flow Metab 2010; 30:923–934.
37. Chu P-L, Keum S, Marchuk DA. A novel genetic locus modulates infarct volume independently of the extent of collateral circulation. Physiol Genomics 2013; 45:751–763.
38. Palmer GM, Ramanujam N. Monte Carlo-based inverse model for calculating tissue optical properties. Part I: theory and validation on synthetic phantoms. Appl Opt 2006; 45:1062–1071.
39. Palmer GM, Viola RJ, Schroeder T, Yarmolenko PS, Dewhirst MW, Ramanujam N. Quantitative diffuse reflectance and fluorescence spectroscopy: tool to monitor tumor physiology in vivo. J Biomed Opt 2009; 14:024010.
40. Cordell RL, Hill SJ, Ortori CA, Barrett DA. Quantitative profiling of nucleotides and related phosphate-containing metabolites in cultured mammalian cells by liquid chromatography tandem electrospray mass spectrometry. J Chromatogr B 2008; 871:115–124.
41. Sinha RA, Farah BL, Singh BK, Siddique MM, Li Y, Wu Y, Ilkayeva OR, Gooding J, Ching J, Zhou J, Martinez L, Xie S, et al. Caffeine stimulates hepatic lipid metabolism by the autophagy-lysosomal pathway in mice. Hepatology 2014; 59:1366–1380.
42. Adams IR, McLaren A. Sexually dimorphic development of mouse primordial germ cells: switching from oogenesis to spermatogenesis. Development 2002; 129:1155–1164.
43. DiNapoli L, Batchvarov J, Capel B. FGF9 promotes survival of germ cells in the fetal testis. Development 2006; 133:1519–1527.
44. Bowles J, Feng C-W, Spiller C, Davidson T-L, Jackson A, Koopman P. FGF9 suppresses meiosis and promotes male germ cell fate in mice. Dev Cell 2010; 19:440–449.
45. Souquet B, Tourpin S, Messiaen S, Moison D, Habert R, Livera G. Nodal signaling regulates the entry into meiosis in fetal germ cells. Endocrinology 2012; 153:2466–2473.
46. Wu Q, Kanata K, Saba R, Deng C-X, Hamada H, Saga Y. Nodal/activin signaling promotes male germ cell fate and suppresses female programming in somatic cells. Development 2013; 140:291–300.
47. Spiller CM, Feng C-W, Jackson A, Gillis AJM, Rolland AD, Looijenga LHJ, Koopman P, Bowles J. Endogenous Nodal signaling regulates germ cell potency during mammalian testis development. Development 2012; 139:4123–4132.
48. Lee JD, Anderson KV. Morphogenesis of the node and notochord: the cellular basis for the establishment and maintenance of left-right asymmetry in the mouse. Dev Dyn 2008; 237:3464–3476.
49. Nagano R, Tabata S, Nakanishi Y, Ohsako S, Kurohmaru M, Hayashi Y. Reproliferation and relocation of mouse male germ cells (gonocytes) during prespermatogenesis. Anat Rec 2000; 258:210–220.
50. Rossi P, Dolci S. Paracrine mechanisms involved in the control of early stages of mammalian spermatogenesis. Front Endocrinol (Lausanne) 2013; 4:181.
51. Sette C, Dolci S, Geremia R, Rossi P. The role of stem cell factor and of alternative c-kit gene products in the establishment, maintenance and function of germ cells. Int J Dev Biol 2000; 44:599–608.
52. Blanco R. A matter of death and life: the significance of germ cell death during spermatogenesis. Int J Androl 1998; 21:236–248.
53. Li J, Savolainen H, Tan F, Zheng S. Orthotopic testicular transplantation in mice. Reproduction 2010; 139:447–452.
54. Reyes JG, Farias JG, Henriquez-Olavarrieta S, Madrid E, Parraga M, Zepeda AB, Moreno RD. The hypoxic testicle: physiology and pathophysiology. Oxid Med Cell Longevity 2012; 2012:15.
55. Brocato J, Chervona Y, Costa M. Molecular responses to hypoxia-inducible factor 1α and beyond. Mol Pharmacol 2014; 85:651–657.
56. Shyh-Chang N, Daley GQ, Cantley LC. Stem cell metabolism in tissue development and aging. Development 2013; 140:2535–2547.
57. Bradbury DA, Simmons TD, Slater KJ, Crouch SPM. Measurement of the ADP: ATP ratio in human leukaemic cell lines can be used as an indicator of cell viability, necrosis and apoptosis. J Immunol Methods 2000; 240: 79–92.
58. Capano M, Crompton M. Bax translocates to mitochondria of heart cells during simulated ischaemia: involvement of AMP-activated and p38 mitogen-activated protein kinases. Biochem J 2006; 395:57–64.
59. Ying W. NAD+/NADH and NADP+/NADPH in cellular functions and

cell death: regulation and biological consequences. Antioxid Redox Signal 2008; 10:179–206.
60. Quail DF, Taylor MJ, Walsh LA, Dieters-Castator D, Das P, Jewer M, Zhang G, Postovit LM. Low oxygen levels induce the expression of the embryonic morphogen Nodal. Mol Biol Cell 2011; 22:4809–4821.
61. Lawrence MG, Margaryan NV, Loessner D, Collins A, Kerr KM, Turner M, Seftor EA, Stephens CR, Lai J, BioResource APC, Postovit L-M, Clements JA, et al. Reactivation of embryonic Nodal signaling is associated with tumor progression and promotes the growth of prostate cancer cells. Prostate 2011; 71:1198–1209.
62. Fulda S, Debatin KM. Extrinsic versus intrinsic apoptosis pathways in anticancer chemotherapy. Oncogene 2006; 25:4798–4811.
63. Dominguez JM II, Davis RT III, McCullough DJ, Stabley JN, Behnke BJ. Aging and exercise training reduce testes microvascular Po2 and alter vasoconstrictor responsiveness in testicular arterioles. Am J Physiol Integr Comp Physiol 2011; 301:R801–R810.
64. Biswas S, Mukherjee R, Tapryal N, Singh AK, Mukhopadhyay CK. Insulin regulates hypoxia-inducible factor-1α transcription by reactive oxygen species sensitive activation of Sp1 in 3T3-L1 preadipocyte. PLoS ONE 2013; 8:e62128.
65. Treins C, Giorgetti-Peraldi S, Murdaca J, Monthouël-Kartmann M-N, Van Obberghen E. Regulation of hypoxia-inducible factor (HIF)-1 activity and expression of HIF hydroxylases in response to insulin-like growth factor I. Mol Endocrinol 2005; 19:1304c1317.
66. Mohyeldin A, Garzon-Muvdi T, Quinones-Hinojosa A. Oxygen in stem cell biology: a critical component of the stem cell niche. Cell Stem Cell 2010; 7:150–161.
67. Ito K, Suda T. Metabolic requirements for the maintenance of self-renewing stem cells. Nat Rev Mol Cell Biol 2014; 15:243–256.
68. Yun JK, McCormick TS, Judware R, Lapetina EG. Cellular adaptive responses to low oxygen tension: apoptosis and resistance. Neurochem Res 1997; 22:517–521.
69. Liao W, Cai M, Chen J, Huang J, Liu F, Jiang C, Gao Y. Hypobaric hypoxia causes deleterious effects on spermatogenesis in rats. Reproduction 2010; 139:1031–1038.
70. Farias JG, Bustos-Obregón E, Orellana R, Bucarey JL, Quiroz E, Reyes JG. Effects of chronic hypobaric hypoxia on testis histology and round spermatid oxidative metabolism. Andrologia 2005; 37:47–52.
71. Motoshima H, Goldstein BJ, Igata M, Araki E. AMPK and cell proliferation–AMPK as a therapeutic target for atherosclerosis and cancer. J Physiol 2006; 574:63–71.
72. Kahn BB, Alquier T, Carling D, Hardie DG. AMP-activated protein kinase: ancient energy gauge provides clues to modern understanding of metabolism. Cell Metab 2005; 1:15–25.
73. Yu S-W, Wang H, Poitras MF, Coombs C, Bowers WJ, Federoff HJ, Poirier GG, Dawson TM, Dawson VL. Mediation of poly(ADP-Ribose) polymerase-1-dependent cell death by apoptosis-inducing factor. Science 2002; 297:259–263.
74. Metcalfe PD, Farivar-Mohseni H, Farhat W, McLorie G, Khoury A, Bagli DJ. Pediatric testicular tumors: contemporary incidence and efficacy of testicular preserving surgery. J Urol 2003; 170:2412–2415.
75. von der Maase H, Rorth M, Walbom-Jorgensen S, Sorensen BL, Christophersen IS, Hald T, Jacobsen GK, Berthelsen JG, Skakkebaek NE. Carcinoma in situ of contralateral testis in patients with testicular germ cell cancer: study of 27 cases in 500 patients. Br Med J (Clin Res Ed) 1986; 293:1398–1401.
76. Naughton CK, Nangia AK, Agarwal A. Varicocele and male infertility: Part II. Pathophysiology of varicoceles in male infertility. Hum Reprod Update 2001; 7:473–481.
77. Cendron M, Huff DS, Keating MA, Snyder HM III, Duckett JW. Anatomical, morphological and volumetric analysis: a review of 759 cases of testicular maldescent. J Urol 1993; 149:570–573.
78. Favorito LA, Sampaio FJB. Testicular migration chronology: do the right and the left testes migrate at the same time? Analysis of 164 human fetuses. BJU Int 2014; 113:650–653.